



1 A Novel Method for Quantifying the Contribution of Regional Transport to PM_{2.5} in Beijing
2 (2013-2020): Combining Machine Learning with Concentration-Weighted Trajectory Analysis

3 Kang Hu¹, Hong Liao¹, Dantong Liu², Jianbing Jin¹, Lei Chen¹, Siyuan Li², Yangzhou Wu³,
4 Changhao Wu⁴, Shitong Zhao², Xiaotong Jiang⁵, Ping Tian^{6,7}, Kai Bi^{6,7}, Ye Wang⁸, Delong
5 Zhao^{6,7}

6 ¹Jiangsu Collaborative Innovation Center of Atmospheric Environment and Equipment
7 Technology, Jiangsu Key Laboratory of Atmospheric Environment Monitoring and Pollution
8 Control, Nanjing University of Information Science & Technology, Nanjing 210044, China.

9 ²Department of Atmospheric Sciences, School of Earth Sciences, Zhejiang University,
10 Hangzhou 310058, China.

11 ³Guangxi Key Laboratory of Environmental Pollution Control Theory and Technology, Guilin
12 University of Technology, Guilin 541004, China.

13 ⁴Institute of International Rivers and Eco-security, Yunnan University, Kunming 650091, China.

14 ⁵College of Biological and Environmental Engineering, Shandong University of Aeronautics,
15 Binzhou, 256600, China.

16 ⁶Beijing Key Laboratory of Cloud, Precipitation and Atmospheric Water Resources, Beijing
17 100089, China.

18 ⁷Field Experiment Base of Cloud and Precipitation Research in North China, China
19 Meteorological Administration, Beijing 100089, China.

20 ⁸Key Laboratory of Meteorological Disaster, Ministry of Education (KLME)/Joint
21 International Research Laboratory of Climate and Environment Change (ILCEC)/
22 Collaborative Innovation Center on Forecast and Evaluation of Meteorological Disasters (CIC-
23 FEMD), Nanjing University of Information Science and Technology, Nanjing 210044, China.

24

25

26 Corresponding author: Hong Liao (hongliao@nuist.edu.cn)

27

28



29 **Abstract**

30 Fine particulate matter (PM_{2.5}) is closely linked to human health, with its sources generally
31 divided into local emissions and regional transport. This study combined concentration-
32 weighted trajectory (CWT) analysis with the HYSPLIT trajectory ensemble to obtain hourly-
33 resolution pollutant source results. The Extreme Gradient Boosting (XGBoost) model was then
34 employed to simulate local emissions and ambient PM_{2.5} in Beijing from 2013 to 2020. The
35 results revealed that clean air masses influencing the Beijing area mainly originated from the
36 north and east regions, exhibiting a strong winter and weak summer pattern. Following the
37 implementation of the Air Pollution Prevention and Control Action Plan (Action Plan) by the
38 Chinese government in 2017, pollution in Beijing decreased significantly, with the most
39 substantial reduction in regional transport pollution events occurring in the west region during
40 summer. Regional transport pollution events were most frequent in spring, up to 1.8 times
41 higher than in winter. Pollutants mainly originated from the west and south regions, while
42 polluted air masses from the east showed the least reduction, and the proportion of pollution
43 sources from this region is gradually increasing. From 2013 to 2020, local emissions were the
44 main contributors of pollution events in Beijing. The Action Plan has more effectively reduced
45 pollution caused by regional transport, particularly during autumn and winter. This finding
46 underscores the importance of Beijing prioritizing local emission reduction while also
47 considering potential contributions from the east region to effectively mitigate pollution events.

48 **Keywords:** Fine particulate matter (PM_{2.5}); concentration-weighted trajectory (CWT);
49 XGBoost model; regional transport

50



51 1. Introduction

52 Ambient fine particulate matter (PM_{2.5}, with particle aerodynamic diameter $\leq 2.5 \mu\text{m}$) is
53 influenced by both natural sources, such as volcanic eruptions, tsunamis, and forest fires, and
54 anthropogenic emissions, including fuel combustion, transportation, and industrial production.
55 Anthropogenic emissions dominate the long-term trend of air pollution (Zhang et al., 2019;
56 Cheng et al., 2019). Numerous epidemiological studies have found that PM_{2.5} can significantly
57 damage human health by exacerbating respiratory and cardiovascular diseases (Bartell et al.,
58 2013; Brauer et al., 2012; Pascal et al., 2014), and also has an impact on weather and climate
59 change (Wang et al., 2014). China's rapid and energy-intensive development over the past
60 several decades has led to severe air pollution and negative public health impacts (Huang et al.,
61 2014). Consequently, controlling pollution and reducing PM_{2.5} concentrations became an urgent
62 issue in China. While meteorological variations caused about 16% of the ambient PM_{2.5} decline
63 during 2013-2017 (Zhang et al., 2019), the uncertainty in reducing PM_{2.5} through
64 meteorological conditions is substantial, and the magnitude of the decrease is not dominated by
65 human actions. Thus, the primary means of controlling PM_{2.5} relies on reducing anthropogenic
66 emissions. To address this issue, the Chinese government implemented the Air Pollution
67 Prevention and Control Action Plan (denoted "Action Plan") from 2013 to 2017 and the Blue
68 Sky Protection Campaign from 2018 to 2020, which effectively controlled anthropogenic
69 emissions and reduced ambient PM_{2.5} concentrations.

70 The concentration of PM_{2.5} can be attributed to local emissions and regional transport. Several
71 methods, such as the HYSPLIT model (Draxler and Rolph, 2010), can be used to distinguish
72 pollutant sources. Wu et al. (Wu et al., 2021) used the HYSPLIT model to simulate the 24-hour
73 backward trajectory in Zhoushan, and identified continental air masses that spent more than 5%
74 of the previous 24 hours over the continent region, while the remaining air masses were
75 identified as oceanic-influenced air masses. Ding et al. (Ding et al., 2019) employed a backward
76 trajectory ensemble to analyze the sources of air masses in Beijing during the study period,
77 finding that air masses with high concentrations of black carbon (BC) mass mainly came from
78 the south and southeast regions. Cluster analysis on backward trajectories can be used to obtain
79 the main direction of aerosols over a period of time, allowing for the analysis and determination
80 of dominant air mass directions. For instance, Li et al. (Li et al., 2022) divided the sources of
81 air masses in the Wuhan area from October to November 2019 into short transport distance,
82 northbound air masses, and regional transport from the northeast and some coastal areas.

83 The HYSPLIT model results are mainly used to view air mass trajectories, making it difficult
84 to directly determine the sources of pollutants. Potential source contribution function (PSCF)
85 and concentration-weighted trajectory (CWT) analyses based on backward trajectories can be
86 used to identify the sources of pollutants through conditional probability results. Hu et al. (Hu
87 et al., 2020) used weighted PSCF to analyze the sources of air masses with different levels of
88 pollution in Beijing and found that polluted air masses from the southwest were an important
89 source of high-level advections during the study period, while light pollution was often
90 accompanied by the regional transport originating from the northeast region. Wu et al. (Wu et
91 al., 2024) used CWT to analyze the sources of pollution in Zhoushan and found that pollutants
92 in Zhoushan are influenced by both local emissions and regional transport. There are no obvious
93 high pollution areas, while in other seasons, PM_{2.5} mainly originates from southern Jiangsu and



94 Shanghai. However, these studies relied on standard HYSPLIT trajectory results, which have
95 lower temporal resolution, limiting the accuracy of pollutant source identification.

96 The Lagrangian air pollution dispersion model, Numerical Atmospheric-dispersion Modelling
97 Environment (NAME) (Jones et al., 2007) can determine the source of polluted air masses by
98 simulating particulate concentrations within each grid point using Monte Carlo methods,
99 followed by 3-D trajectories of plume basins. Liu et al. (Liu et al., 2020) used the NAME model
100 to study the sources of air masses in Beijing during the winter of 2019 and divided them into
101 local emissions and regional transport to analyze the convective mixing process of BC under
102 the influence of local emissions. However, due to limitations in computing resources, the
103 NAME model is difficult to use for obtaining long-term emission source analysis results.

104 Multiple methods can be used to predict $PM_{2.5}$ concentrations, such as statistical models (e.g.,
105 linear mixed-effect models and generalized additive models) (Fang et al., 2016; Ma et al., 2016),
106 chemical transport model (CTM)-based algorithms (Geng et al., 2015; Kong et al., 2021),
107 physical models (Lin et al., 2018), and recently emerging machine learning models, including
108 Extreme Gradient Boosting (XGBoost) and Random Forest (Liang et al., 2020; Wei et al., 2021;
109 Xiao et al., 2018; Xue et al., 2019; Huang et al., 2021). Geng et al. (Geng et al., 2021) used
110 satellite observations of aerosol optical depth (AOD) and meteorological data combined with
111 the XGBoost model to explore the long-term variations of $PM_{2.5}$ caused by changes in
112 meteorological conditions from 2000 to 2018. Kleine Deters et al. (Kleine Deters et al., 2017)
113 demonstrated the relevance of statistical models based on machine learning for predicting $PM_{2.5}$
114 concentrations from meteorological data. This method of predicting aerosol concentrations
115 using only meteorological data has been widely used (Asadollahfardi et al., 2016; Zeng et al.,
116 2021). For instance, Grange et al. (Grange et al., 2018) used meteorological data, synoptic scale,
117 planetary boundary layer height (PBLH), and time variables to explain daily PM_{10}
118 concentrations in Switzerland. In summary, machine learning models have achieved high
119 accuracy in estimating and predicting $PM_{2.5}$ concentrations and have high use value, and the
120 rise of machine learning methods has also provided feasibility for quantifying the contribution
121 of regionally transported air masses.

122 In this study, we combined CWT analysis with the HYSPLIT trajectory ensemble to obtain
123 hourly-resolution $PM_{2.5}$ source results and used this approach to distinguish between local
124 emissions and regional transport. Predictive XGBoost models were developed for Beijing using
125 meteorological data and time variables to explain local and ambient $PM_{2.5}$ concentrations. By
126 combining these two methods, the contribution of regional transport to $PM_{2.5}$ in Beijing can be
127 quantified.

128

129 **2. Materials and methods**

130 **2.1 Site and instrumentation**

131 The $PM_{2.5}$ data (Fig. 1a) were obtained from in situ air quality monitoring conducted by the
132 China National Environmental Monitoring Center from 2013 to 2020. The monitoring station
133 is located in Haidian Wanliu (39.96°N, 116.29°E), situated in the central urban area of Beijing.



134 Meteorological data, including temperature, relative humidity, pressure, precipitation, wind
135 speed, and PBLH, were sourced from the European Centre for Medium-Range Weather
136 Forecasts (ECMWF) ERA5 hourly reanalysis dataset
137 (<https://cds.climate.copernicus.eu/datasets>).

138

139 2.2 Air mass source

140 The air mass trajectory data were obtained from the $1^\circ \times 1^\circ$ horizontal and vertical wind fields
141 of the Global Data Assimilation System (GDAS) reanalysis products
142 (<ftp://arlftp.arlhq.noaa.gov/pub/archives/gdas1>), available every 3 hours. The HYSPLIT
143 trajectory ensemble was used to generate 27 equally probable 24-hour backward air mass
144 trajectories for the target point (39.96°N, 116.29°E, 250 m a.s.l.) in every hour by using PySplit
145 (Cross, 2015). Given the equal probability of air masses being transported to the target point
146 for each trajectory in the HYSPLIT trajectory ensemble, a conditional probability CWT
147 analysis was applied to determine the hourly source area of pollution.

148 In the CWT analysis method, each grid point is assigned a weight (equation 2), and the
149 contribution of each grid point to the pollutant concentration at the target site is calculated using
150 the air mass residence time and pollutant concentration (Hopke et al., 1993; Polissar et al., 1999;
151 Xu and Akhtar, 2010) (equation 1). The grid point resolution was set to $0.25^\circ \times 0.25^\circ$ for this
152 study. In equations 1, C_{ij} is the average weighted concentration at grid point (i, j), l is the
153 trajectory index, M represents the total number of trajectories, C_l is the $PM_{2.5}$ concentration
154 corresponding to the target site, and τ_{ijl} is the residence time of trajectory l passing through
155 the grid point. In calculation, the number of trajectories falling on each grid point is used instead
156 of the residence time.

$$157 \quad C_{ij} = \frac{\sum_{l=1}^M C_l \times \tau_{ijl}}{\sum_{l=1}^M \tau_{ijl}} \times W(n_{ij}) \quad (1)$$

$$158 \quad W(n_{i,j}) = \begin{cases} 1.00, & 3n_{ave} < n_{ij} \\ 0.70, & 1.5n_{ave} < n_{ij} \leq 3n_{ave} \\ 0.40, & n_{ave} < n_{ij} \leq 1.5n_{ave} \\ 0.17, & n_{ij} < n_{ave} \end{cases} \quad (2)$$

159 where n_{ij} represents the number of trajectories that fall within the grid point, and n_{ave}
160 represents the average number of trajectories passing through each grid point.

161 The potential source contribution to $PM_{2.5}$ at the target site was investigated by segregating the
162 region where the backward air masses had passed into five parts: local (which is a region around
163 central Beijing, 115.3~117.5°E, 39.4~41°N); north region (the northern plateau at 108~117.5°E,
164 41~43°N); west region (the western plateau at 108~115.3°E, 34~41°N); south region (the
165 southern plain at 115.3~120°E, 34~39.4°N); and east region (the eastern plain at 117.5~120°E,
166 39.4~43°N). The concentration is integrated over each grid point in each segregated region
167 obtained from the CWT analysis, and the contributions of each air mass fraction are obtained.
168 The region with the highest contribution is used to determine the dominant source of air masses
169 in Beijing at each time, classifying the overall air mass sources into local emissions (Fig. 1g)
170 and regional transport (Fig. 1h).



171

172 2.3 Deriving the long-term local emission and ambient PM_{2.5}

173 An XGBoost model is employed to derive the local and ambient PM_{2.5} results. The
174 hyperparameters used in the model include the maximum number of boosting iterations,
175 learning rate, maximum depth of a tree, minimum sum of instance weight needed in a child,
176 subsampling ratio of a training instance, and subsampling ratio of columns when constructing
177 each tree. The input parameters for the XGBoost model comprise meteorological variables
178 (temperature, relative humidity, wind speed, surface pressure, and precipitation) and temporal
179 parameters (year, month, day of the week, and day of the year), as referenced from Xu et al.
180 (Xu et al., 2023). Additionally, PBLH, which has been shown to significantly impact pollutant
181 concentrations in previous observational (Su et al., 2018; Miao and Liu, 2019; Miao et al., 2019)
182 and machine learning studies (Xiao et al., 2021; Li et al., 2017b; Shen et al., 2018), was included
183 as an input parameter. For the machine learning process, data from 2013 to 2019 were used for
184 training the XGBoost models, while data from 2020 were used for model validation.

185 The relatively small proportion of high-concentration PM_{2.5} can lead to underestimation of
186 high-concentration events in the model results (Wei et al., 2020). To address this issue, a high
187 PM_{2.5} indicator was defined as a daily average PM_{2.5} concentration exceeding the monthly
188 average plus twice the standard deviation. In this study, original high PM_{2.5} indicators accounted
189 for 6% of the data points during the period dominated by local and ambient PM_{2.5}. To balance
190 the proportion of high-concentration PM_{2.5} in the entire database, the Synthetic Minority Over-
191 sampling Technique (SMOTE) (Torgo, 2011) was applied during data preprocessing. SMOTE
192 artificially generates new synthetic samples along the line between high-concentration data
193 points and their selected nearest neighbors, effectively oversampling the high-concentration
194 data. As a result, the proportion of high PM_{2.5} indicators increased to 21% and 22% for local
195 and ambient PM_{2.5}, respectively.

196 Hyperparameter optimization and performance evaluation of the model were conducted using
197 fivefold cross-validation (CV). In this approach, 20% of the data is randomly selected for model
198 testing, while the remaining 80% is used for training. This process is repeated five times,
199 ensuring that each record is used once as testing data. The coefficient of determination (r^2) was
200 employed to assess the correlation between the XGBoost model predictions and observed
201 values, while the root mean square error (RMSE) was used as a performance evaluation statistic.
202 After obtaining the relation between the input parameters and PM_{2.5}, we are able to derive the
203 hourly local and ambient PM_{2.5} once all long-term input parameters (Fig. S2).

204 3 Results and discussion

205 3.1 Evaluation of the XGBoost PM_{2.5} prediction model

206 During the model validation process, the XGBoost model results for ambient PM_{2.5} (Fig. 2a2)
207 demonstrated an r^2 of 0.74 and an RMSE of 20 $\mu\text{g m}^{-3}$ when compared to observations. The
208 XGBoost model results for local PM_{2.5} exhibited an r^2 of 0.78 and an RMSE of 21 $\mu\text{g m}^{-3}$. An
209 analysis of the PM_{2.5} frequency distribution in Beijing revealed a strong agreement between the



210 XGBoost model results and observations for both ambient and local $PM_{2.5}$. As illustrated in Fig.
211 S1, local and ambient $PM_{2.5}$ in Beijing display a distinct seasonal variation, with higher values
212 in winter and lower values in summer. However, the transport of clean air masses from the
213 north diminishes the seasonal variation characteristics of ambient $PM_{2.5}$ in Beijing, making
214 winter pollution less prominent compared to other seasons.

215 Fig. S2 reveals that ambient pollution events ($PM_{2.5} > 75 \mu g m^{-3}$) in Beijing are primarily
216 influenced by air masses originating from the south and west, particularly under the control of
217 westward air masses. With the exception of December (Fig. 3b1), westward air masses often
218 bring higher monthly average $PM_{2.5}$ to Beijing. Air masses originating from the south region
219 can also transport more pollutants to Beijing (Fig. S2). However, unlike the high-frequency
220 polluted air masses from the west, southward air masses are associated with higher $PM_{2.5}$
221 concentrations, particularly during autumn and winter (Fig. 3c1). This phenomenon can be
222 attributed to the higher pollution levels in Hebei and Shandong provinces compared to Beijing
223 during these seasons, as verified by AOD observations from Moderate Resolution Imaging
224 Spectroradiometer (MODIS) on the Aqua satellites over Eastern China (Zhang and Reid, 2010;
225 Hu et al., 2018) (Fig. S4). Notably, in contrast to westward transport, air masses from the south
226 region in February predominantly exhibited a cleaning effect on Beijing, even before 2017 (Fig.
227 S2b). This can be explained by the occurrence of these transport processes during or shortly
228 after the Spring Festival, a period characterized by extremely low anthropogenic emissions,
229 resulting in lower ambient $PM_{2.5}$ compared to local emissions in the megacity of Beijing.
230 Following the implementation of the Action Plan, the polluted air masses from the south region
231 transitioned from carrying higher $PM_{2.5}$ to levels close to local emission concentrations in
232 Beijing, leading to a more equal contribution to pollution and clean events in the area (Fig.
233 S3c1).

234 3.2 Impact of clean air masses from transported regions on $PM_{2.5}$ in Beijing

235 In this study, clean air masses are defined as those associated with ambient $PM_{2.5}$ in the Beijing
236 area that are lower than the concentrations resulting from local emissions, as illustrated below
237 the dashed line in Fig. 3a1-d1. This study reveals that clean air masses predominantly originate
238 from the east and north regions during the period 2013-2020, which is consistent with previous
239 studies (Zhang et al., 2018; Hu et al., 2020). Clean air masses from different directions exhibit
240 similar seasonal variations in their ability to reduce locally emitted pollution in Beijing, with a
241 strong reduction effect in winter and a weaker effect in summer (Fig. 3a2-d2). This
242 phenomenon is closely related to the seasonal variations in pollutant emissions. Due to the
243 combined influence of increased residential emissions from heating activities and
244 meteorological conditions in Beijing during autumn and winter, local $PM_{2.5}$ in Beijing presents
245 higher concentrations. Consequently, the influx of clean air masses results in a more
246 pronounced reduction in $PM_{2.5}$ during these seasons. The weaker attenuation effect of $PM_{2.5}$
247 transported from the south region during December and January can be attributed to the high-
248 frequency and high-concentration pollution contributions from air masses originating in this
249 region during this period.



250 Due to a significant reduction in anthropogenic emissions after 2017, the attenuation of $PM_{2.5}$
251 concentrations by clean air masses from all directions was significantly lower than before 2017
252 (Fig. S5a2-d2). Compared to the period prior to 2017, the mean attenuation of $PM_{2.5}$
253 concentrations in Beijing decreased by 3, 10, 3, and $7 \mu\text{g m}^{-3}$ ($p < 0.01$) for air masses
254 originating from the north, west, south, and east regions, respectively.

255 3.3 Variations in Beijing $PM_{2.5}$ concentrations under transport-induced pollution events

256 Transport-induced pollution events in Beijing are defined as the occurrence of ambient $PM_{2.5}$
257 exceeding both local $PM_{2.5}$ and the light pollution standard ($75 \mu\text{g m}^{-3}$). Fig. 4a1-d1 demonstrate
258 that the monthly variation of $PM_{2.5}$ in Beijing generally follows a unimodal pattern, with higher
259 values in winter and lower values in summer, except when under the influence of eastern air
260 mass transport. This phenomenon is closely related to the seasonal variations in anthropogenic
261 emissions in China and the characteristics of climate change (Renhe et al., 2014; Li et al., 2017a;
262 Zhang et al., 2015). The overall $PM_{2.5}$ in Beijing under the influence of eastward pollution air
263 masses exhibits a bimodal distribution, with frequent high-concentration pollution events
264 occurring in January and October. Even after the effective control of anthropogenic emissions
265 in 2017, a second peak of high-concentration pollution persists in October (Fig. 4d2). Fig. 4a2-
266 d2 illustrate the effectiveness of the Action Plan in controlling pollutant concentrations in the
267 Beijing area. Since 2017, $PM_{2.5}$ in Beijing has been significantly lower than the values observed
268 before 2017 during transport-induced pollution events. Moreover, during January and from
269 June to September, there were periods when the regional transport of polluted air masses from
270 a fixed direction did not contribute to pollution events in Beijing.

271 An analysis of the proportion of transport-induced pollution events from different regions in
272 Beijing (Fig. 5) shows that after the implementation of the Action Plan in 2017, the number of
273 pollution events dominated by regional transport decreased significantly. From spring to winter
274 (defined as January-February and December of the same year in this study), the largest decrease
275 in transport-induced pollution events occurred in the north, west, west and south regions in each
276 season, with the lowest decrease occurring in the east region during winter. Among all regions,
277 the east region exhibited the smallest decrease in transport-induced pollution events. This is
278 likely due to the fact that eastward air masses have already been contributing a significant
279 amount of clean air to the region.

280 The temporal variation in the number of transport-induced pollution events from different
281 regions (Fig. S6) revealed that air masses transported from the west region contributed to the
282 most frequent pollution events in each season except summer. The highest number of events
283 occurred in spring 2016 (322), autumn 2016 (375), and winter 2017 (308). Summer transport-
284 induced pollution events were mainly influenced by polluted air masses transported from the
285 south, with a gradual decrease in the number of events over the years. Although pollution events
286 in Beijing primarily occur in autumn and winter, this study found that after 2017, the season
287 when Beijing was most affected by transport-induced pollution events was spring, contributing
288 a total of 685 pollution events, while autumn and winter contributed 266 and 392 events,
289 respectively. The impact of polluted air masses on summer transport was minimal, with only
290 215 occurrences.



291 Fig. 5a shows that in spring, transport-induced pollution events in Beijing were mainly
292 dominated by polluted air masses transported from the west and south. The highest proportion
293 of regional transport events from the west occurred in 2016, reaching 68%, while the highest
294 proportion of southward transport-induced pollution events occurred in spring 2020. The
295 increased frequency of pollution air masses transported from the south after 2017 can be
296 attributed to the effective control of anthropogenic emissions, resulting in a decrease in PM_{2.5}
297 transported from various regions, especially from westward sources (Fig. S6a). The decrease
298 in the proportion of pollution events transported from the west, which originally accounted for
299 a large proportion, led to an increase in the contribution of remaining incoming air masses to
300 Beijing.

301 Before 2017, transport-induced pollution events in Beijing during summer were mainly
302 affected by polluted air masses from the south. Even in 2015, when the proportion of transport-
303 induced pollution events from south region was lowest during the entire period, it still
304 accounted for 50% of the total number of transport-induced pollution events that year. However,
305 after the implementation of the Action Plan, the proportion of transport-induced pollution
306 events from the south region gradually decreased from 57% to 25%. Meanwhile, pollution air
307 masses originating from the east increasingly dominated the occurrence of pollution events in
308 Beijing.

309 Transport-induced pollution events in Beijing mainly originated from the west and had the
310 highest contribution proportion in autumn before 2019 (except for 2013, when the contribution
311 proportion was 34%, second only to southward air masses at 35%). After 2019, the contribution
312 of eastward air masses became dominant in autumn. In winter, polluted air masses from the
313 west were the main source of transport-induced pollution events. In 2020, the east region,
314 previously believed to contribute significant amounts of clean air, substantially contributed to
315 transport-induced pollution events across various seasons. This finding may prompt Beijing to
316 prioritize emission reduction in the east region when implementing future joint prevention and
317 control measures.

318 **4 Conclusion**

319 This study combined a machine learning method and Concentration-Weighted Trajectory
320 (CWT) analysis to derive local emissions and ambient observed PM_{2.5} in Beijing from 2013 to
321 2020, thus the contribution of regional transport to PM_{2.5} in Beijing can be quantified. The
322 impact of clean air masses (defined as those with ambient PM_{2.5} concentrations lower than local
323 emissions) mainly originated from the east and north regions. These clean air masses from
324 different directions exhibited similar seasonal variations in their ability to reduce ambient
325 pollution in Beijing, with a stronger reduction effect in winter and a weaker reduction effect in
326 summer.

327 Except for the regional transport from the east region, the seasonal variation of PM_{2.5} in Beijing
328 under the influence of transport-induced pollution events (ambient PM_{2.5} exceeding both local
329 PM_{2.5} and 75 μg m⁻³) shows a general trend of high concentrations in winter and low
330 concentrations in summer. The main reason for this phenomenon is related to the seasonal



331 emissions of pollutants in China and the characteristics of climate change. Before 2019, the
332 west region was the primary source of pollution events during autumn and winter. However,
333 starting from 2019, the east region became the main contributor of polluted air masses in
334 autumn. Additionally, among all regions, the east region exhibited the smallest decrease in
335 transport-induced pollution events after 2017.

336 From 2013 to 2020, local emissions were the main contributors to pollution events in Beijing.
337 However, the Air Pollution Prevention and Control Action Plan, implemented by the Chinese
338 government in 2017, more effectively mitigated pollutants caused by regional transport
339 compared to local emissions, particularly during autumn and winter. This finding suggests that
340 Beijing should prioritize reducing local emissions while also accounting for potential
341 contributions from the east region in its future pollution prevention and control strategies.

342

343 **Code and data availability**

344 The Machine learning code is archived on Zenodo at <https://doi.org/10.5281/zenodo.13994450>,
345 while the CWT code is archived on Zenodo at <https://doi.org/10.5281/zenodo.13994400>. The
346 meteorology and PM_{2.5} data used in this study can be accessed at
347 <https://dx.doi.org/10.17632/bhfktx3kz8.2>.

348

349 **Author contribution**

350 Kang Hu, Hong Liao and Dantong Liu designed and carried out the experiments. Kang Hu
351 wrote the code and final paper with contributions from all other authors. Hong Liao, Dantong
352 Liu, Lei Chen and Jianbing Jin reviewed and edited the paper.

353

354 **Competing interests**

355 The contact author has declared that none of the authors has any competing interests.

356

357 **Acknowledgements**

358 This research was supported by the China Postdoctoral Science Foundation (2023M741773),
359 Postdoctoral Fellowship Program of CPSF (GZC20231150).

360

361 **Reference**



- 362 Asadollahfardi, G., Madinejad, M., Aria, S. H., and Motamadi, V.: Predicting Particulate Matter
363 (PM_{2.5}) Concentrations in the Air of Shahr-e Ray City, Iran, by Using an Artificial Neural
364 Network, *Environmental Quality Management*, 25, 71-83, 2016.
- 365 Bartell, S. M., Longhurst, J., Tjoa, T., Sioutas, C., and Delfino, R. J.: Particulate air pollution,
366 ambulatory heart rate variability, and cardiac arrhythmia in retirement community residents
367 with coronary artery disease, *Environmental health perspectives*, 121, 1135-1141, 2013.
- 368 Brauer, M., Amann, M., Burnett, R. T., Cohen, A., Dentener, F., Ezzati, M., Henderson, S. B.,
369 Krzyzanowski, M., Martin, R. V., and Van Dingenen, R.: Exposure assessment for estimation
370 of the global burden of disease attributable to outdoor air pollution, *Environmental science &
371 technology*, 46, 652-660, 2012.
- 372 Cheng, N., Cheng, B., Li, S., and Ning, T.: Effects of meteorology and emission reduction
373 measures on air pollution in Beijing during heating seasons, *Atmospheric Pollution Research*,
374 10, 971-979, 2019.
- 375 Cross, M.: PySPLIT: a Package for the Generation, Analysis, and Visualization of HYSPLIT
376 Air Parcel Trajectories, *SciPy*, 133-137,
- 377 Ding, S., Zhao, D., He, C., Huang, M., He, H., Tian, P., Liu, Q., Bi, K., Yu, C., and Pitt, J.:
378 Observed interactions between black carbon and hydrometeor during wet scavenging in mixed-
379 phase clouds, *Geophysical Research Letters*, 46, 8453-8463, 2019.
- 380 Draxler, R. and Rolph, G.: HYSPLIT (HYbrid Single-Particle Lagrangian Integrated Trajectory)
381 model access via NOAA ARL READY website (<http://ready.arl.noaa.gov/HYSPLIT.php>).
382 NOAA Air Resources Laboratory, Silver Spring, MD, 25, 2010.
- 383 Fang, X., Zou, B., Liu, X., Sternberg, T., and Zhai, L.: Satellite-based ground PM_{2.5} estimation
384 using timely structure adaptive modeling, *Remote Sensing of Environment*, 186, 152-163, 2016.
- 385 Geng, G., Zhang, Q., Martin, R. V., van Donkelaar, A., Huo, H., Che, H., Lin, J., and He, K.:
386 Estimating long-term PM_{2.5} concentrations in China using satellite-based aerosol optical
387 depth and a chemical transport model, *Remote sensing of Environment*, 166, 262-270, 2015.
- 388 Geng, G., Xiao, Q., Liu, S., Liu, X., Cheng, J., Zheng, Y., Xue, T., Tong, D., Zheng, B., and
389 Peng, Y.: Tracking air pollution in China: near real-time PM_{2.5} retrievals from multisource
390 data fusion, *Environmental Science & Technology*, 55, 12106-12115, 2021.
- 391 Grange, S. K., Carslaw, D. C., Lewis, A. C., Boleti, E., and Hueglin, C.: Random forest
392 meteorological normalisation models for Swiss PM₁₀ trend analysis, *Atmospheric Chemistry
393 and Physics*, 18, 6223-6239, 2018.



- 394 Hopke, P. K., Gao, N., and Cheng, M.-D.: Combining chemical and meteorological data to infer
395 source areas of airborne pollutants, *Chemometrics and Intelligent Laboratory Systems*, 19, 187-
396 199, 1993.
- 397 Hu, K., Kumar, K. R., Kang, N., Boiyo, R., and Wu, J.: Spatiotemporal characteristics of
398 aerosols and their trends over mainland China with the recent Collection 6 MODIS and OMI
399 satellite datasets, *Environmental Science and Pollution Research*, 25, 6909-6927, 2018.
- 400 Hu, K., Zhao, D., Liu, D., Ding, S., Tian, P., Yu, C., Zhou, W., Huang, M., and Ding, D.:
401 Estimating radiative impacts of black carbon associated with mixing state in the lower
402 atmosphere over the northern North China Plain, *Chemosphere*, 252, 126455, 2020.
- 403 Huang, C., Hu, J., Xue, T., Xu, H., and Wang, M.: High-resolution spatiotemporal modeling for
404 ambient PM_{2.5} exposure assessment in China from 2013 to 2019, *Environmental Science &
405 Technology*, 55, 2152-2162, 2021.
- 406 Huang, R.-J., Zhang, Y., Bozzetti, C., Ho, K.-F., Cao, J.-J., Han, Y., Daellenbach, K. R., Slowik,
407 J. G., Platt, S. M., and Canonaco, F.: High secondary aerosol contribution to particulate
408 pollution during haze events in China, *Nature*, 514, 218-222, 2014.
- 409 Jones, A., Thomson, D., Hort, M., and Devenish, B.: The UK Met Office's next-generation
410 atmospheric dispersion model, NAME III, in: *Air pollution modeling and its application XVII*,
411 Springer, 580-589, 2007.
- 412 Kleine Deters, J., Zalakeviciute, R., Gonzalez, M., and Rybarczyk, Y.: Modeling PM_{2.5} urban
413 pollution using machine learning and selected meteorological parameters, *Journal of Electrical
414 and Computer Engineering*, 2017, 5106045, 2017.
- 415 Kong, L., Tang, X., Zhu, J., Wang, Z., Li, J., Wu, H., Wu, Q., Chen, H., Zhu, L., and Wang, W.:
416 A 6-year-long (2013–2018) high-resolution air quality reanalysis dataset in China based on the
417 assimilation of surface observations from CNEMC, *Earth System Science Data*, 13, 529-570,
418 2021.
- 419 Li, M., Zhang, Q., Kurokawa, J.-i., Woo, J.-H., He, K., Lu, Z., Ohara, T., Song, Y., Streets, D.
420 G., and Carmichael, G. R.: MIX: a mosaic Asian anthropogenic emission inventory under the
421 international collaboration framework of the MICS-Asia and HTAP, *Atmospheric Chemistry
422 and Physics*, 17, 935-963, 2017a.
- 423 Li, S., Liu, D., Kong, S., Wu, Y., Hu, K., Zheng, H., Cheng, Y., Zheng, S., Jiang, X., and Ding,
424 S.: Evolution of source attributed organic aerosols and gases in a megacity of central China,
425 *Atmospheric Chemistry and Physics Discussions*, 2022, 1-19, 2022.
- 426 Li, T., Shen, H., Yuan, Q., Zhang, X., and Zhang, L.: Estimating ground-level PM_{2.5} by fusing
427 satellite and station observations: a geo-intelligent deep learning approach, *Geophysical
428 Research Letters*, 44, 11,985-911,993, 2017b.



- 429 Liang, F., Xiao, Q., Huang, K., Yang, X., Liu, F., Li, J., Lu, X., Liu, Y., and Gu, D.: The 17-y
430 spatiotemporal trend of PM_{2.5} and its mortality burden in China, *Proceedings of the National
431 Academy of Sciences*, 117, 25601-25608, 2020.
- 432 Lin, C., Liu, G., Lau, A. K. H., Li, Y., Li, C., Fung, J. C. H., and Lao, X. Q.: High-resolution
433 satellite remote sensing of provincial PM_{2.5} trends in China from 2001 to 2015, *Atmospheric
434 environment*, 180, 110-116, 2018.
- 435 Liu, D., Hu, K., Zhao, D., Ding, S., Wu, Y., Zhou, C., Yu, C., Tian, P., Liu, Q., and Bi, K.:
436 Efficient vertical transport of black carbon in the planetary boundary layer, *Geophysical
437 Research Letters*, 47, e2020GL088858, 2020.
- 438 Ma, Z., Hu, X., Sayer, A. M., Levy, R., Zhang, Q., Xue, Y., Tong, S., Bi, J., Huang, L., and Liu,
439 Y.: Satellite-based spatiotemporal trends in PM_{2.5} concentrations: China, 2004–2013,
440 *Environmental health perspectives*, 124, 184-192, 2016.
- 441 Miao, Y. and Liu, S.: Linkages between aerosol pollution and planetary boundary layer structure
442 in China, *Science of the Total Environment*, 650, 288-296, 2019.
- 443 Miao, Y., Li, J., Miao, S., Che, H., Wang, Y., Zhang, X., Zhu, R., and Liu, S.: Interaction
444 between planetary boundary layer and PM_{2.5} pollution in megacities in China: a Review,
445 *Current Pollution Reports*, 5, 261-271, 2019.
- 446 Pascal, M., Falq, G., Wagner, V., Chatignoux, E., Corso, M., Blanchard, M., Host, S., Pascal,
447 L., and Larrieu, S.: Short-term impacts of particulate matter (PM₁₀, PM_{10–2.5}, PM_{2.5}) on
448 mortality in nine French cities, *Atmospheric Environment*, 95, 175-184, 2014.
- 449 Polissar, A., Hopke, P., Paatero, P., Kaufmann, Y., Hall, D., Bodhaine, B., Dutton, E., and Harris,
450 J.: The aerosol at Barrow, Alaska: long-term trends and source locations, *Atmospheric
451 Environment*, 33, 2441-2458, 1999.
- 452 Renhe, Z., Li, Q., and Zhang, R.: Meteorological conditions for the persistent severe fog and
453 haze event over eastern China in January 2013, *Science China Earth Sciences*, 57, 26-35, 2014.
- 454 Shen, H., Li, T., Yuan, Q., and Zhang, L.: Estimating regional ground-level PM_{2.5} directly
455 from satellite top-of-atmosphere reflectance using deep belief networks, *Journal of Geophysical
456 Research: Atmospheres*, 123, 13,875-813,886, 2018.
- 457 Su, T., Li, Z., and Kahn, R.: Relationships between the planetary boundary layer height and
458 surface pollutants derived from lidar observations over China: regional pattern and influencing
459 factors, *Atmospheric Chemistry and Physics*, 18, 15921-15935, 2018.
- 460 Torgo, L.: *Data mining with R: learning with case studies*, Chapman and Hall/CRC2011.



- 461 Wang, Y., Wang, M., Zhang, R., Ghan, S. J., Lin, Y., Hu, J., Pan, B., Levy, M., Jiang, J. H., and
462 Molina, M. J.: Assessing the effects of anthropogenic aerosols on Pacific storm track using a
463 multiscale global climate model, *Proceedings of the National Academy of Sciences*, 111, 6894-
464 6899, 2014.
- 465 Wei, J., Li, Z., Lyapustin, A., Sun, L., Peng, Y., Xue, W., Su, T., and Cribb, M.: Reconstructing
466 1-km-resolution high-quality PM_{2.5} data records from 2000 to 2018 in China: spatiotemporal
467 variations and policy implications, *Remote Sensing of Environment*, 252, 112136, 2021.
- 468 Wei, J., Li, Z., Cribb, M., Huang, W., Xue, W., Sun, L., Guo, J., Peng, Y., Li, J., Lyapustin, A.,
469 Liu, L., Wu, H., and Song, Y.: Improved 1 km resolution PM_{2.5} estimates across China using
470 enhanced space–time extremely randomized trees, *Atmos. Chem. Phys.*, 20, 3273-3289,
471 10.5194/acp-20-3273-2020, 2020.
- 472 Wu, Y., Liu, D., Wang, X., Li, S., Zhang, J., Qiu, H., Ding, S., Hu, K., Li, W., and Tian, P.:
473 Ambient marine shipping emissions determined by vessel operation mode along the East China
474 Sea, *Science of The Total Environment*, 769, 144713, 2021.
- 475 Xiao, Q., Chang, H. H., Geng, G., and Liu, Y.: An ensemble machine-learning model to predict
476 historical PM_{2.5} concentrations in China from satellite data, *Environmental science &
477 technology*, 52, 13260-13269, 2018.
- 478 Xiao, Q., Zheng, Y., Geng, G., Chen, C., Huang, X., Che, H., Zhang, X., He, K., and Zhang,
479 Q.: Separating emission and meteorological contributions to long-term
480 PM_{2.5} trends over eastern China during 2000–2018, *Atmospheric
481 Chemistry and Physics*, 21, 9475-9496, 10.5194/acp-21-9475-2021, 2021.
- 482 Xu, R., Ye, T., Yue, X., Yang, Z., Yu, W., Zhang, Y., Bell, M. L., Morawska, L., Yu, P., and
483 Zhang, Y.: Global population exposure to landscape fire air pollution from 2000 to 2019, *Nature*,
484 621, 521-529, 2023.
- 485 Xu, X. and Akhtar, U.: Identification of potential regional sources of atmospheric total gaseous
486 mercury in Windsor, Ontario, Canada using hybrid receptor modeling, *Atmospheric Chemistry
487 and Physics*, 10, 7073-7083, 2010.
- 488 Xue, T., Zheng, Y., Tong, D., Zheng, B., Li, X., Zhu, T., and Zhang, Q.: Spatiotemporal
489 continuous estimates of PM_{2.5} concentrations in China, 2000–2016: A machine learning
490 method with inputs from satellites, chemical transport model, and ground observations,
491 *Environment international*, 123, 345-357, 2019.
- 492 Zeng, Z., Gui, K., Wang, Z., Luo, M., Geng, H., Ge, E., An, J., Song, X., Ning, G., and Zhai,
493 S.: Estimating hourly surface PM_{2.5} concentrations across China from high-density
494 meteorological observations by machine learning, *Atmospheric Research*, 254, 105516, 2021.



495 Zhang, J. and Reid, J.: A decadal regional and global trend analysis of the aerosol optical depth
496 using a data-assimilation grade over-water MODIS and Level 2 MISR aerosol products,
497 Atmospheric Chemistry and Physics, 10, 10949-10963, 2010.

498 Zhang, L., Wang, T., Lv, M., and Zhang, Q.: On the severe haze in Beijing during January 2013:
499 Unraveling the effects of meteorological anomalies with WRF-Chem, Atmospheric
500 Environment, 104, 11-21, 2015.

501 Zhang, L., Zhao, T., Gong, S., Kong, S., Tang, L., Liu, D., Wang, Y., Jin, L., Shan, Y., and Tan,
502 C.: Updated emission inventories of power plants in simulating air quality during haze periods
503 over East China, Atmospheric Chemistry and Physics, 18, 2065-2079, 2018.

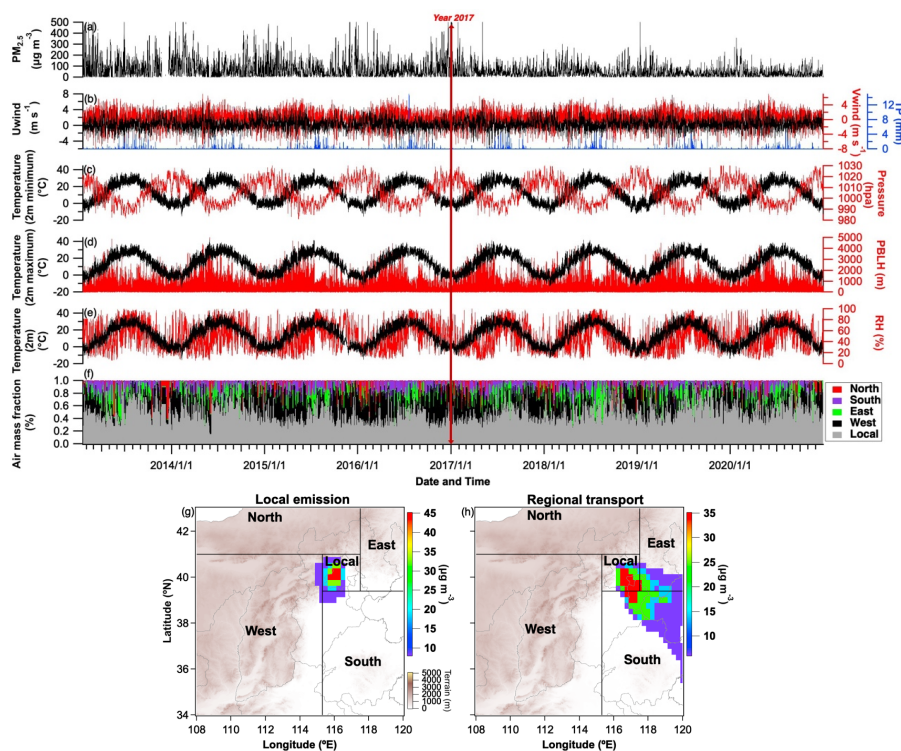
504 Zhang, Q., Zheng, Y., Tong, D., Shao, M., Wang, S., Zhang, Y., Xu, X., Wang, J., He, H., and
505 Liu, W.: Drivers of improved PM_{2.5} air quality in China from 2013 to 2017, Proceedings of
506 the National Academy of Sciences, 116, 24463-24469, 2019.

507

508



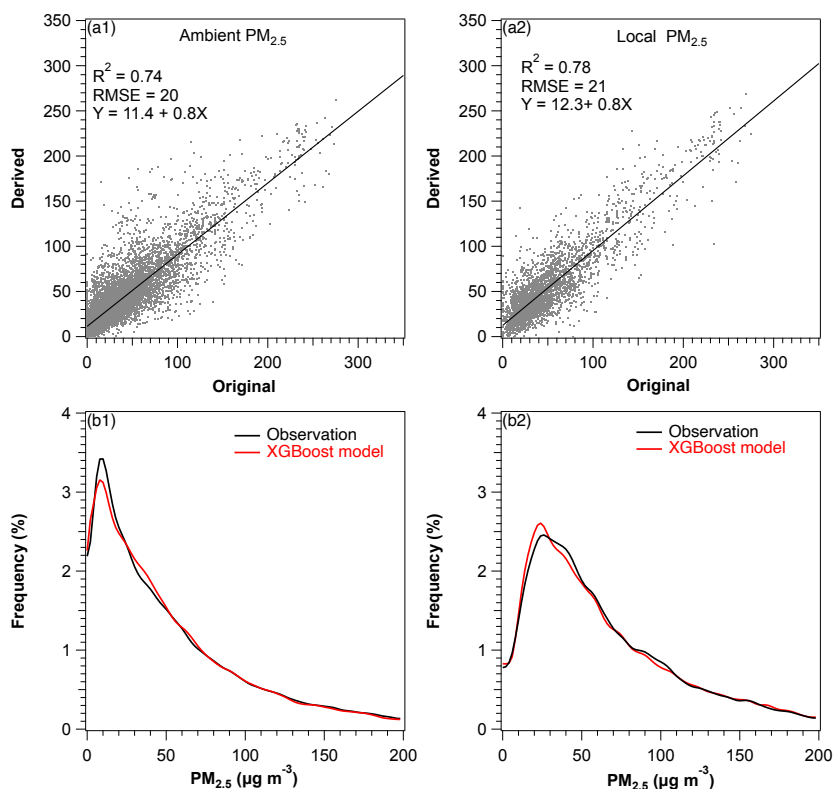
509 **Figures and captions**



510

511 Fig. 1. Temporal evolution of parameters used in the XGBoost model: (a) $PM_{2.5}$; (b) U-wind,
512 V-wind, and total precipitation; (c) 2-m minimum temperature and surface pressure; (d) 2-m
513 maximum temperature and planetary boundary layer height; (e) 2-m temperature and relative
514 humidity; (f) air mass fraction in contributing sources derived from the Concentration-
515 Weighted Trajectory (CWT) model for a 1-day backward trajectory. The red vertical line with
516 arrows indicates the implementation of environmental regulations. Typical examples of the
517 CWT model analysis are shown for (g) a local emission period (25 August 2013) and (h) a
518 regional transport period (15 July 2013).

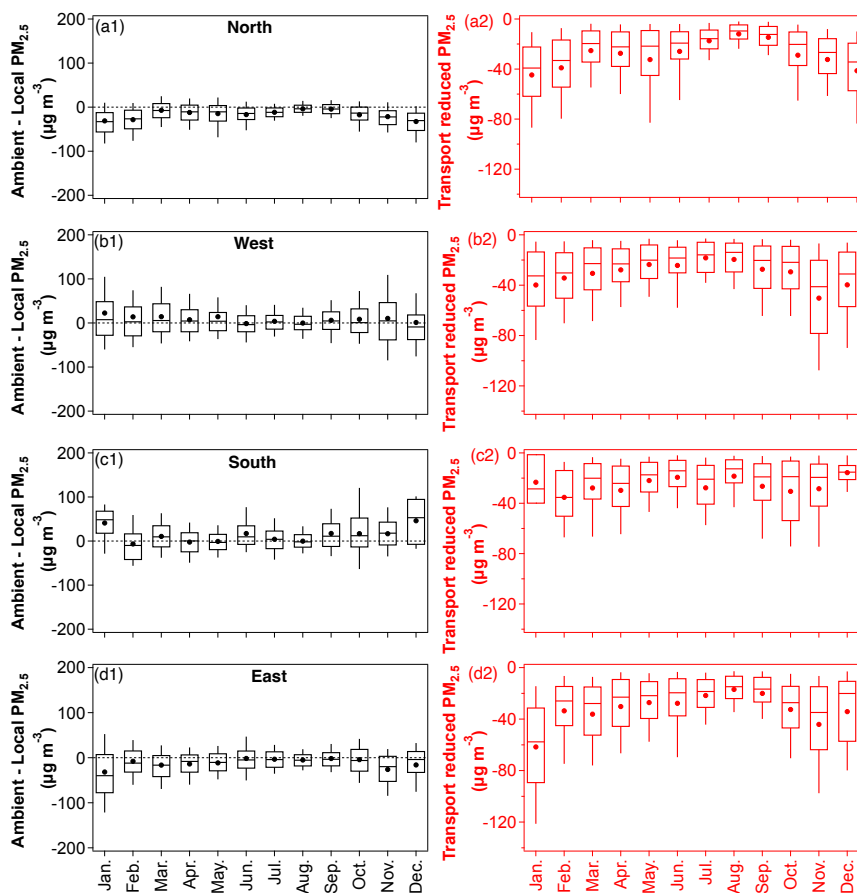
519



520

521 Fig. 2. Comparison of XGBoost model estimates and measurements for (a1) ambient $PM_{2.5}$ and
522 (a2) local $PM_{2.5}$ using testing samples from 2020. Frequency distributions of $PM_{2.5}$ observations
523 (black lines) and XGBoost model predictions (red lines) obtained through fivefold cross-
524 validation for (b1) ambient $PM_{2.5}$ and (b2) local $PM_{2.5}$.

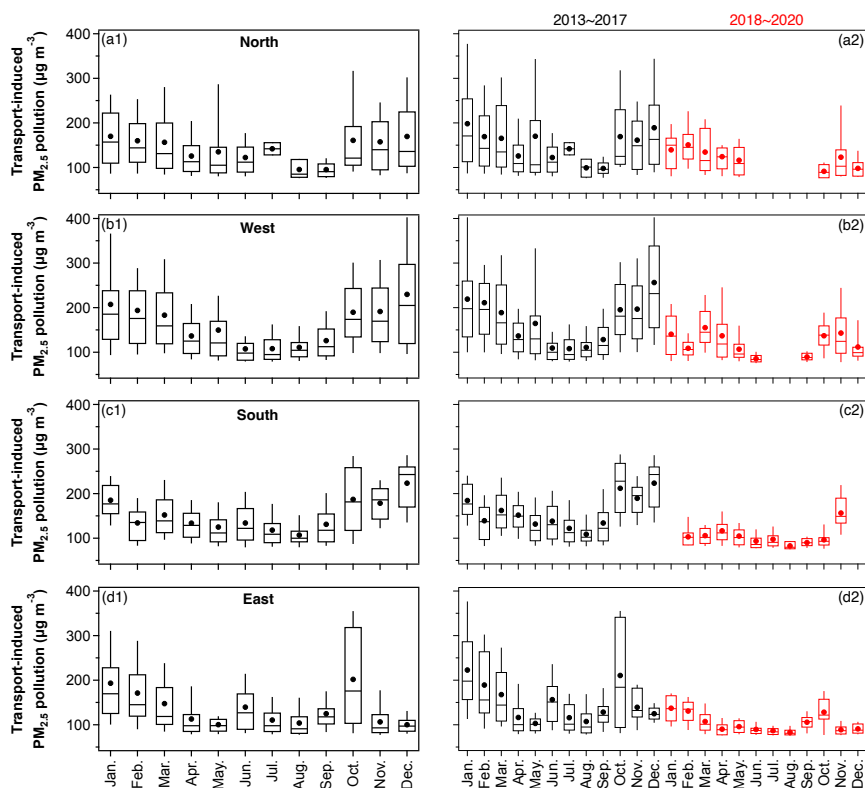
525



526

527 Fig. 3. Monthly variations of the difference between ambient and local PM_{2.5} from the (a1)
528 North, (b1) West, (c1) South, and (d1) East regions. Right panels show monthly variations of
529 PM_{2.5} reductions caused by regional transport for the corresponding source regions in the left
530 panels. The upper and lower boundaries represent the 75th and 25th percentiles, respectively,
531 while the solid origin represents the average value.

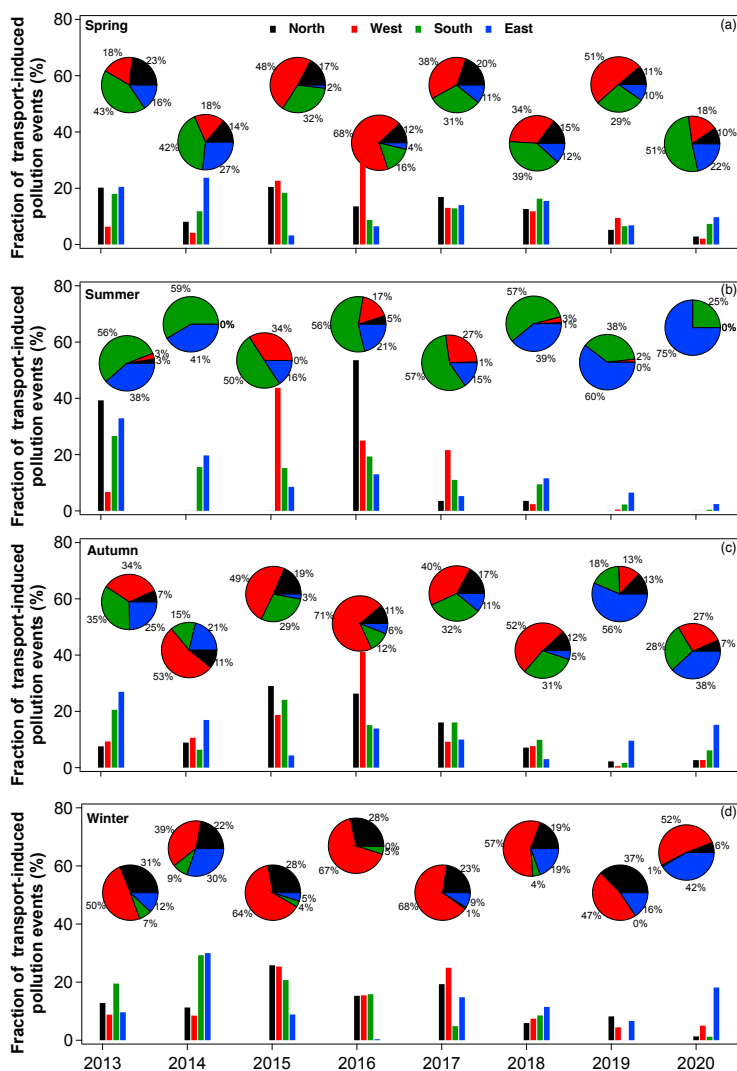
532



533

534 Fig. 4. Monthly variations of transport-induced $PM_{2.5}$ pollution (ambient $PM_{2.5}$ exceeding local
535 $PM_{2.5}$ and $75 \mu g m^{-3}$) from the (a1) North, (b1) West, (c1) South, and (d1) East regions during
536 2013-2020. Right panels show monthly variations of transport-induced $PM_{2.5}$ pollution before
537 (black) and after (red) 2017 for the corresponding source regions in the left panels. The upper
538 and lower boundaries represent the 75th and 25th percentiles, respectively, while the solid origin
539 represents the average result.

540



541

542 Fig. 5. Histograms depict the annual fraction of transport-induced pollution events in each
543 direction relative to the total number of occurrences from 2013 to 2020 during (a) spring, (b)
544 summer, (c) autumn, and (d) winter. Pie charts illustrate the proportion of transport-induced
545 pollution events in each direction for each year within the corresponding seasons.

546